World Conference on
Timber Engineering
Oslo 2023

ROTATIONAL STIFFNESS OF NEWLY DEVELOPED LVL-BASED COLUMN-HEAD REINFORCEMENT FOR POINT-SUPPORTED SLAB-COLUMN BUILDING SYSTEMS

Cristóbal Tapia[1], Felix Amtsberg[2], Aaron Münzer[3], Simon Aicher[4], Achim Menges[5]

ABSTRACT: The paper presents a recently developed concept for the transmission of vertical loads between columns in point-supported timber slab systems. The concept consists of a specially milled beech LVL element inserted into the end of a GLT column, thus allowing to receive concentrated loads from an also specially milled LVL pin element. Under axial compression the LVL insert proved being able to redistribute the compression stresses effectively before transferring the stresses to the lower GLT column. This paper investigates the rotational stiffness of this concept, both numerically and experimentally with two manufactured specimens. For the studied geometry the obtained rotational stiffness was 3.4×10^2 kNm/rad, being in good agreement with the finite element simulations. Relevant aspects of the robotic manufacturing relating to the tight tolerances needed are discussed.

KEYWORDS: multi-storey timber buildings, GLT, beech LVL, rotational stiffness, robotic manufacturing, point-supports

1 INTRODUCTION

The construction of high-rise buildings based on modern wood engineered products has been a reality for the past decade, with the number of new projects steadily rising worldwide (see e.g. [2, 11]). This development has been fostered by a variety of interacting factors, associated with mechanical, environmental, architectonic and social aspects. Timber, having an excellent weight/strength ratio and enabling a high degree of prefabrication for rapid on-site assembly, fits perfectly the needs of multi-storey building construction. Furthermore, the increasing urge to transit to more CO_2-neutral building technologies has lead to an increasing interest in timber—a natural CO_2 container—as a viable option for high-rise buildings, up until now almost exclusively dominated by reinforced concrete and steel.

This relatively new field of multi-storey timber buildings has not come free of challenges, mostly represented by the need for new performant, bespoken connection solutions for the different components. Examples of problematic joints are found especially in column-slab type of structures, typically consisting of glued laminated timber (GLT) columns and cross-laminated timber (CLT) plates with an additional lateral bracing system. Here, the point-support situation leads to highly demanding requirements for the connection system. In such a situation two main problems arise: firstly, the point-support condition of the plate induces high shear and bending stresses in the immediate region of the CLT surrounding the column. This poses a problem for the CLT plate due to its relative low rolling strength values, normally about three times lower than the shear strength of timber parallel to the fiber. Secondly, the vertical load originating from the upper floors and carried by the upper column needs to be transferred to the bottom column supporting the CLT plate. Owed to the low compressive strength perpendicular to the grain of timber, $f_{c,90}$, the column cannot be supported directly on the CLT plate, and therefore the column force is normally transferred through a hole in the CLT plate (e.g. [10, 11]). This further worsens the stress situation in the CLT in the column region, as tensile stress concentrations will develop in the vicinity of the hole on the bending tension side [13]. Solutions for the reinforcement of CLT plates under these loading conditions are implemented or have been proposed in [10, 13, 18].

The transfer of the vertical loads has been addressed by Fast et al. [11] for columns at the edges of the CLT plate and in [10] for columns placed at the inner field of the CLT plate. In both cases the concept applied to transfer the vertical loads is very similar, consisting on a cylindrical steel profile used to transfer the loads through the reduced cross-section of the column. This steel profile has attached at both ends steel plates, which are fixed to the columns.

[1]Materials Testing Institute (MPA), University of Stuttgart, Pfaffenwaldring 4b, 70569 Stuttgart, Germany, cristobal.tapia-camu@mpa.uni-stuttgart.de
[2]Institute for Computational Design and Construction (ICD), University of Stuttgart, Keplerstraße 11, 70174 Stuttgart, Germany, felix.amtsberg@icd.uni-stuttgart.de
[3]Materials Testing Institute (MPA), University of Stuttgart, Pfaffenwaldring 4b, 70569 Stuttgart, Germany, simon.aicher@mpa.uni-stuttgart.de
[4]Materials Testing Institute (MPA), University of Stuttgart, Pfaffenwaldring 4b, 70569 Stuttgart, Germany, aaron.muenzer@mpa.uni-stuttgart.de
[5]Institute for Computational Design and Construction (ICD), University of Stuttgart, Keplerstraße 11, 70174 Stuttgart, Germany, achim.menges@icd.uni-stuttgart.de

https://doi.org/10.52202/069179-0094

The efficacy of these solutions has been verified by means of full-sized experimental campaigns, for example in [4], where also two additional concepts were tested. Nevertheless, as mentioned in [4], the inclusion of the special steel connectors is costly and alternatives should be explored that require less steel.

Within the context of Research Project 3 of the Cluster of Excellence "Integrative Computational Design and Construction for Architecture" (IntCDC), at the University of Stuttgart, the problem of timber connections for multi-storey timber buildings was addressed. One of the specific objectives was to develop an almost pure timber column-to-column connection. The concept leverages modern digital fabrication methods to combine and glue different timber products with the required tolerances (≈ 1 mm), enabling complex geometries for an efficient use of material and transfer of loads. This paper presents first experimental and finite element results on the newly developed connection concept. Especially, the behavior under vertical and lateral load situations is analyzed, and manufacturing aspects will be discussed.

2 DESCRIPTION OF THE CONNECTION CONCEPT

2.1 GEOMETRY

The newly developed connection consists of an assemblage of three specially milled timber components as illustrated in Fig. 1. The load coming from the top GLT column is first transferred to a stepped, pyramid-shaped beech laminated veneer lumber (LVL) element embedded in an equal negatively shaped pyramid cavity in the column. Then the load is transferred to a hardwood pin element with a similar stepped geometry. From there, the load travels to the bottom column through the same, but inverted, beech LVL component.

The number and dimensions of the steps of each component is variable. The radius, r, of the milled corners (see Fig. 2) is bound to the diameter of the used milling tool, which for the studied case was $r = 8$ mm.

The idea behind the chosen geometry for the beech LVL insert is to enable a gradual transfer of stresses from the smaller cross-section of the pin element to the GLT column. In other words, the stronger LVL insert serves as transition zone for the spreading of the compressive stresses, which are then transferred to the column. The same principle applies to the geometry of the hardwood pin element.

2.2 MATERIALS

In terms of used materials, it is evident that the pin element, owed to its reduced cross-section, is subjected to higher compression stresses as the GLT column. Thus, a strong material is required. For the present study, unidirectional, CE-marked beech LVL according to EN 14374 [7] was used for this component. According to the producer's Declaration of Performance [14] the characteristic compressive strength parallel to grain can be assumed as $57.5 \times 1.2 = 69$ MPa for use in service class 1. However, it should be noted that the performed experiments suggest that an even stronger material—e.g. from tropical hardwoods or densified veneer wood—is required to fully utilize the connection. Similarly, the transition pyramid-shaped insert element is also subjected to rather high stresses, reason for which beech LVL was used as well. The LVL blocks from which the pyramid insert elements were milled consisted of block-glued LVL plates.

Each component is glued into the next one by means of a two-component polyurethane adhesive. For a proper functioning of the connection, the different elements must fit precisely into each other. Otherwise, the loads would concentrate on a subset of the contact surfaces, leading to premature local damage and reducing the capacity of the connection. Small gaps can be effectively bridged by the used gap-filling adhesive, however only to a certain degree. Therefore, it is essential to achieve very small tolerances (< 1 mm) during the manufacturing process. The components can easily be pre-assembled, leaving only one last on-site bonding step per connection during the construction phase.

Due to the geometry of the LVL pyramid insert, stresses perpendicular to the grain are expected in the column. In order to avoid an early failure due to splitting, the GLT column can be reinforced by means of self-tapping screws. The effect of this reinforcement measure was experimentally studied in [17], where a Weibull-based design approach is presented, and will not be further addressed in this paper.

2.3 BEHAVIOR UNDER AXIAL COMPRESSION LOADING

The column was previously investigated numerically and experimentally under axial compression in [17]. In

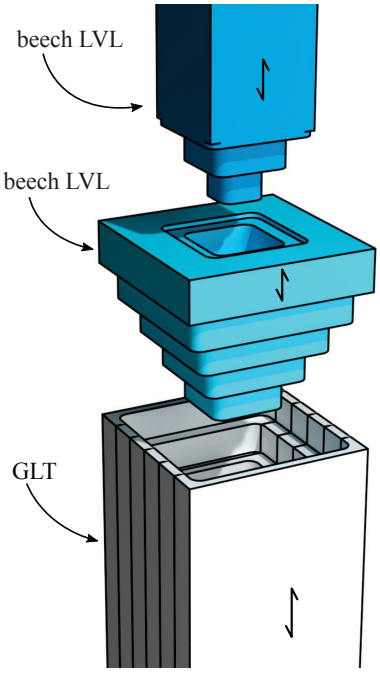

Figure 1: *Concept for the proposed connection for the vertical transfer of loads from upper columns*

https://doi.org/10.52202/069179-0094

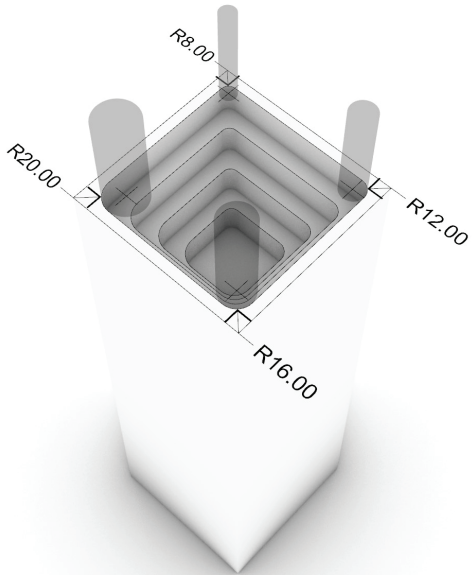

Figure 2: *Example of an automatically generated column detail based on 4 different milling tool diameters*

that study, a series of five specimens was manufactured and tested in order to obtain maximum capacities and to understand the failure mode under axial compression, where the load was introduced exclusively through the LVL pin element. The specimens had identical dimensions as those presented in this paper. The general concept of the connection can be understood by looking at Fig. 3a, where the stresses in the z-direction obtained by a 3D finite element (FE) model are shown.

The rather concentrated load coming from the LVL pin on the top induces a region of high stresses directly below the pin element. However, by placing a strong material in this region—in this case beech LVL aligned vertically—, the stresses can be taken and spread downwards. By using the special stepped geometry, the high stresses can be kept inside the LVL insert, roughly following the stress-isolines as shown in Fig. 3a. The σ_z stresses at the interface between LVL insert and GLT column can be accurately estimated by an analytical model, making this a suitable tool for the design of the connection, without requiring a full 3D FE model [17].

A further analyzed issue was the formation of a region of tensile stresses perpendicular to the fiber, directly below the LVL insert, as illustrated in Fig. 3b. The experiments showed that these stresses were responsible for the failure of the specimens, as splitting triggered the maximum capacity of all tested specimens. The consideration of these stresses was tackled in a first approximation by a Weibull-based design approach, similar as done in [3]. However, local crushing in the GLT, directly underneath the LVL insert was also observed. Therefore, the exact failure model is owed most likely to a more complex combination of compression and splitting stresses.

A further analysis was also made to assess the influence of the application of loads directly on the top surface of the LVL insert, simulating a CLT plate being supported by

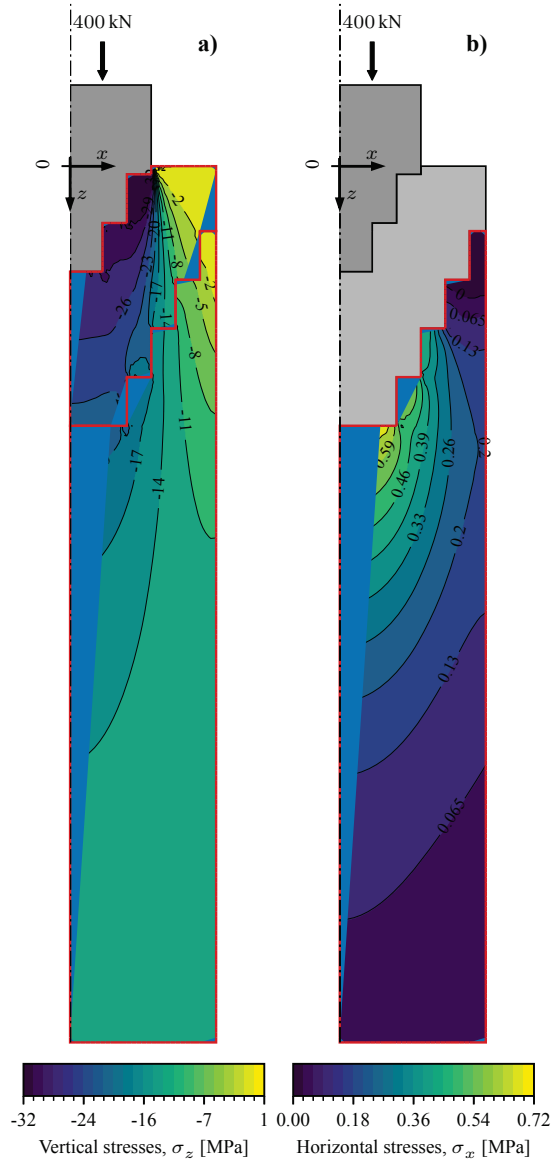

Figure 3: *Contour plots of vertical stresses σ_z (a) and horizontal stresses σ_x (b) for a load of* 400 kN *applied on top of the LVL pin element*

the column. The numerical results showed that the vertical stresses, σ_z, were rather evenly distributed and that the splitting stresses, σ_x, decreased by a factor of two to three.

2.4 MANUFACTURING CONSIDERATIONS

In the digital process chain, parametric models were developed specifically to produce the design details of the outlined column-to-column connections. These allowed an effortless generation of the geometry and resulting milling paths to produce and test various configurations of, for example, the column cross-section steps. Other parameters that were automatically generated include the infeed and path planning according to the selected cutter geometry and blank, feed rate and speed. Rhinoceros 6 [12] and Grasshopper were used as the development environment

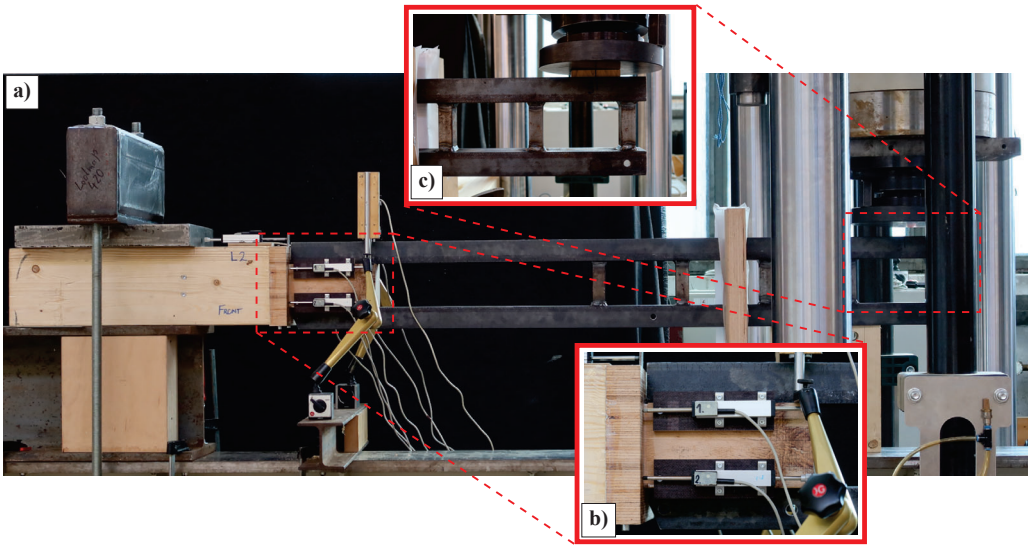

Figure 4: *Example of the realized experimental set-up for the lateral loading testing of the connection concept*

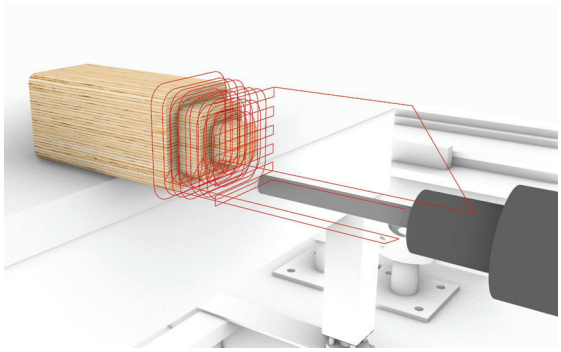

Figure 5: *Rhino Model of the geometry and automatically generated toolpath (red)*

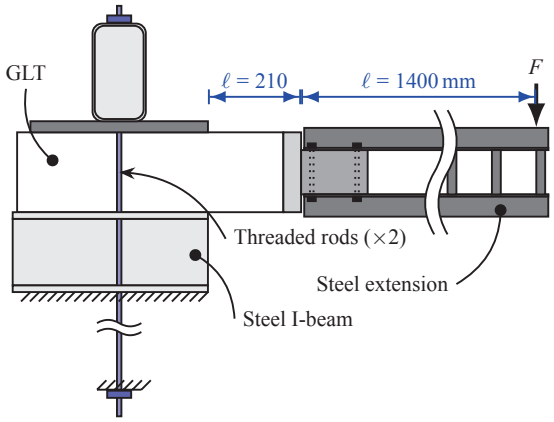

Figure 6: *Experimental setup for the lateral loading configuration*

for tool path, NC code generation and simulation. The data were then transferred to KUKA-CNC and implemented (see Fig. 5).

3 EXPERIMENTAL INVESTIGATIONS

3.1 STUDIED CONFIGURATIONS

The reported connection was studied under lateral loading in order to obtain the moment capacity, as well as the rotational stiffness. The specimens are composed of a softwood GLT column with a cross-section of 180 mm × 180 mm and a length of 600 mm; the dimensions of the LVL insert and the pin elements are described in [17]. The specimens of both configurations were tested at the Division of Timber Constructions of the Materials Testing Institute, University of Stuttgart, with a servo-hydraulic machine with a maximum loading capacity of 1.6 MN. The load was applied in displacement-controlled manner with a stroke rate of 1.5 mm/sec until failure occurred. Since the achieved loads were rather small compared to the maximum capacity of the machine (about 2 kN compared to 1.6 MN), the data recording was accompanied by a significant amount of electronic noise. Future experiments will use an independent load measuring cell, appropriate for the expected load range.

The experimental set-up with its relevant dimensions is illustrated in Fig. 6. Here, an extension made from two steel profiles welded together was attached to the LVL pin element by means of threaded rods. This increases the lever arm, thus increasing the moment to shear force ratio on the connection. The steel extension had a total weight of 14.2 kg. The specimens were clamped to a large steel profile, to achieve a cantilever situation, as presented in Fig. 4.

In both configurations the specimens were reinforced by means of full-threaded self-tapping screws. This was done in order to delay splitting due to stresses perpendicular to the grain. The position of the used screws can be seen in Fig. 7.

https://doi.org/10.52202/069179-0094

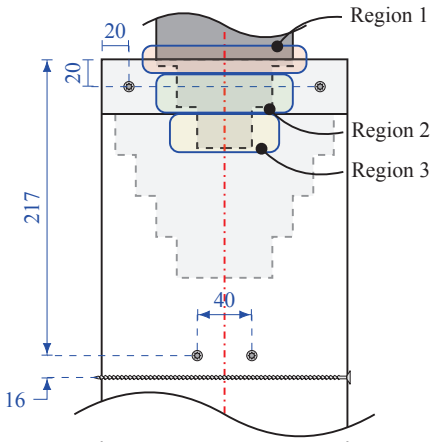

Figure 7: *Position of screws used to reinforce the connection during the lateral loading experiments and definition of regions in the interface between LVL-insert and LVL-pin elements (dimensions in millimeter)*

3.2 MANUFACTURE OF PROTOTYPES

The fabrication setup used to produce the joints from softwood GLT and beech LVL consists of a KUKA 420 R3031 industrial robot mounted on a KUKA KL 4000 linear axis with a travel distance of 11 m. The system is designed and tested for a machining accuracy of $\leq$ 0.4 mm. An air-cooled HSD 929L spindle with a power of 14.40 kW was used for subtractive machining. The column-to-column connection was produced using a coated spiral roughing/finishing cutter with a useful length of 30 mm, a total length of 205 mm and a diameter of 16 mm. After three tests with varying step geometries a total of 12 assemblies were fabricated for experimental testing. The GLT column and LVL pin were machined horizontally (see Fig. 8), while the LVL pocket element was manufactured vertically (see Fig. 9). These were also reclamped to be machined on both sides. Other parameters are feed rate (3000 mm/min GLT, 600 mm/min LVL), speed (12 000 rpm), final infeed (0.25 mm) and offset (0.25 mm). The bond line thickness resulting from this milling set-up was analyzed on a parallel milled sample using an electronic stereo microscope [5]. Predominantly thin (<1 mm) bond line thicknesses were observed. The mean glue joint thickness and the corresponding coefficient of variation were 0.14 mm and 40 % respectively (see Fig. 10). This indicates a high accuracy of the milling process and that, if necessary, the programmed tolerances could be further reduced.

3.3 RESULTS

3.3.1 General observed behavior and failure mode

Figure 11 shows the global moment-displacement curve of specimens L1 and L2 (displacement as machine piston displacement). Both specimens presented a linear behavior until about 1.5 kNm, where first audible failure noise could be heard. This is clearly shown in Fig. 11 for specimen L2, but not for specimen L1. The reason for this is that for the case of specimen L1 this initial failure occurred during the first attempt of testing this specimen, which had to be

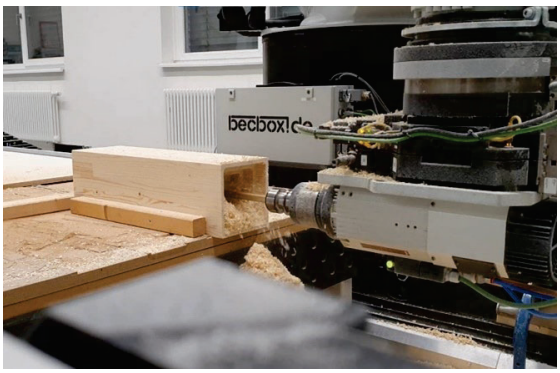

Figure 8: *Horizontal milling of the GLT column*

Figure 9: *Vertical milling of the LVL pocket*

interrupted, as the used steel extension proved to have a far too low shear stiffness—initially both steel profiles were held together exclusively by threaded rods, which were then welded together to increase the shear stiffness.

After the first load drop-down a second failure took place. A further increase in the load triggered the global failure at about M_1 = 2.57 kNm and M_2 = 2.46 kNm for specimens L1 and L2, respectively. Beyond this point the upper part of the pin element began to visibly to be pulled out from the cavity of the LVL insert (see Fig 12). A summary of the achieved maximum loads and corresponding moments is presented in Table 1.

The first can most probably be attributed to the failure of the interface between LVL-pin and LVL-insert elements

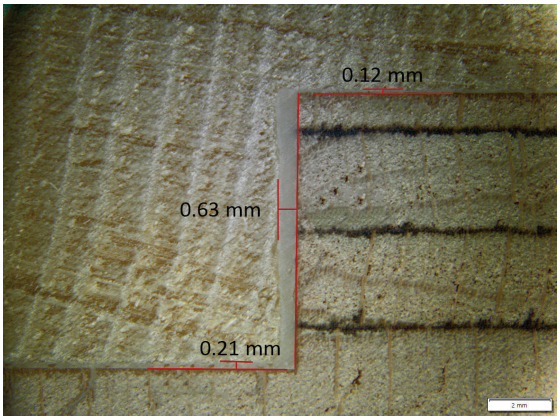

Figure 10: *Adhesive joint thickness of a milled sample*

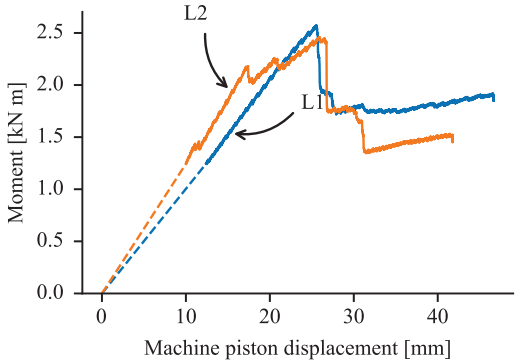

Figure 11: *Load-displacement curves of both tested specimens.*

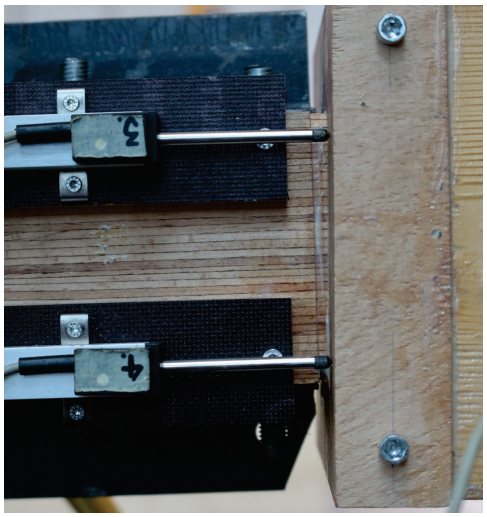

Figure 12: *Pin element of specimen L1 being pulled-out of the LVL insert after reaching maximum load.*

in the vertical surfaces of region 1 shown in Fig. 7. As the damage progressed, the horizontal faces in region 1 failed, causing the second load drop. Finally, the vertical and horizontal bond faces of region 2 failed, causing the global failure of the connection. The bond faces of region 3 probably failed together with those of region 2, as they show a smaller total area to transfer the loads and the lever arm is smaller compared to region 2, thus increasing the bending stresses. Figure 13 shows the failed vertical surface of region 2 for Specimen L1, where a rather low percentage of fiber breakage can be observed.

Table 1: *Maximum loads and moments achieved by specimens L1 and L2, and estimated rotational stiffness*

Specimen	Maximum Load [kN]	Maximum Moment [kN m]	Rotational Stiffness [kNm/rad]
L1	1.84	2.57	3.4×10^2
L2	1.76	2.46	–

Figure 13: *Shear failure on the vertical surface of region 2, corresponding to the vertical surface of the second step of the LVL-pin element*

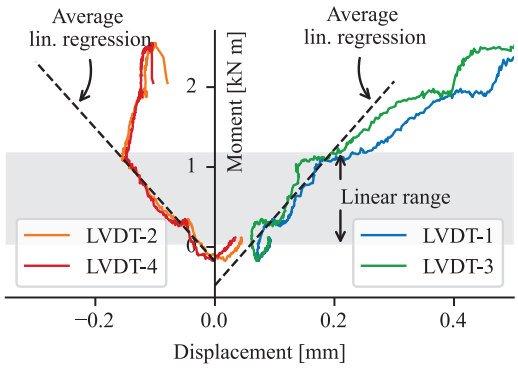

Figure 14: *Measured relative displacement between pin element and LVL insert of specimen L1. LVDT's 1 and 3: tension side; LVDT's 2 and 4: compression side. Grey region marks the load limits used to compute the average linear regression on both sides.*

3.3.2 LVDT measurements

Figure 14 presents the moment-displacement curves for the LVDT's which measure the displacements in the tension (1 and 3) and compression (2 and 4) regions of specimen L1. Although the data is rather noisy, the expected behavior of positive and negative displacements in the tension and compression regions, respectively, can be clearly observed. The dashed lines in Fig. 14 represent the linear regression of the averaged curves from LVDT's in tension and compression within the linear range denoted by the shaded region.

The corresponding measurements from Specimen L2 are not presented here, as problems with the fixation of the steel extension lever arm caused a relative shift between steel and pin-element, resulting in erroneous data. Future experiments will consider a more robust concept for the clamping of the steel extension to the LVL-pin element.

3.3.3 Rotational stiffness

The rotational stiffness of the connection can be obtained from the LVDT measurements at positions 1 and 3 (bending tension side), and 2 and 4 (bending compression side), as shown in Fig 14. To estimate the rotational stiffness, k_θ, the rotation angle between the LVL-insert and the LVL-pin

https://doi.org/10.52202/069179-0094

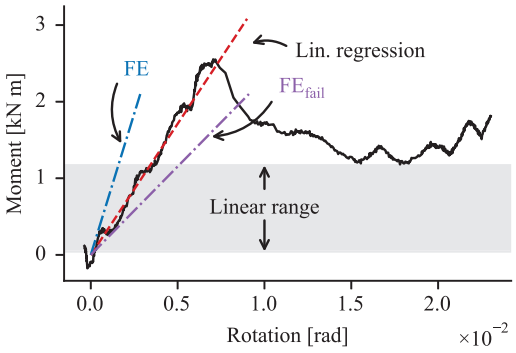

Figure 15: *Moment-rotation-rotation curve computed for specimen L1. The rotation was computed from the averaged results of the front and rear LVDT's*

elements was computed as

$$\theta = \arctan\left(\frac{\bar{u}_t - \bar{u}_c}{d}\right), \tag{1}$$

where $\bar{u}_t$ and $\bar{u}_c$ are the averages of the displacements measured in tension and compression, respectively, and d is the vertical distance between the LVDT's, in this case $d = 80$ mm.

Figure 15 shows the moment-rotation curve obtained for Specimen L1, from which the rotational stiffness can be estimated by means of a linear regression. The linear regression was computed for the data within the linear range defined in Fig. 14. Finally, a rotational stiffness $k_\theta = 3.43 \times 10^2$ kNm/rad was obtained for Specimen L1.

4 NUMERICAL ANALYSIS

4.1 DESCRIPTION OF FE MODEL

A parametric 3D finite element model was programmed in Abaqus V2022 [1] with the available Python API. The model consists of three parts (GLT column, LVL insert and LVL pin) bonded by means of cohesive interactions on the respective vertical faces and contact behavior for the horizontal surfaces (i.e. end grain can take up compressive loading but not tension). This can be seen in Fig. 16, where the different cohesive and contact regions, as well as the used mesh is shown. Symmetry along the YZ-plane was used to reduce the total number of elements. The boundary conditions corresponding to the clamping where applied on the side surfaces according to Fig. 6, by restraining all degrees of freedom. The load was applied as a shear force-moment pair on a reference point placed at the center of the top face of the LVL pin part. This reference point controls a rigid surface, which is "tied" to the top face of the pin.

The geometry was meshed with linear 3D brick elements with incompatible modes of type C3D8I, with an approximate size of 3 mm. The elastic material properties used are shown in Table 2, while the cohesive interaction was defined with stiffness parameters $k_{nn} = k_{tt} = 1000$ N/mm^3, with finite sliding. A failure of the bond line of the vertical surfaces of region 1 (see Fig. 7), in the bending tension

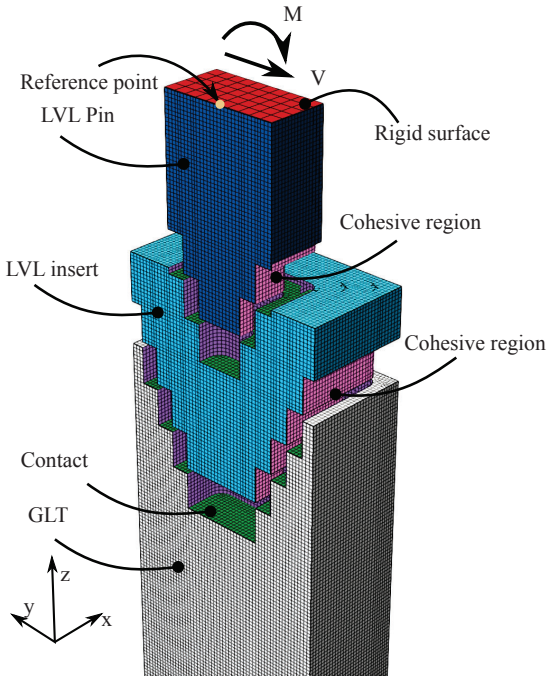

Figure 16: *Illustration of the FE mesh, together with the definition of cohesive regions and load application*

Table 2: *Elastic material stiffness properties used for the FEM simulations*

Material	E_0* [MPa]	E_{90} [MPa]	ν_{12} [–]	ν_{23} [–]	G [MPa]	G_r [MPa]
CLT[1)]	11 000	370	0.2	0.02	690	50
LVL[2)]	12 800	2000	0.2	0.02	430	43

[1)] acc. to values in [8] for softwood boards strength class C24 as indicated in [9]

[2)] acc. to values in [6, 19] (except ν_{ij})

* E_0: MOE parallel to fiber; E_{90}: MOE perpendicular to fiber; G: shear modulus; G_r: rolling shear modulus; $\nu_{12} = \nu_{13}$: Poisson coefficient between the fiber direction and the other two orthogonal directions; ν_{23} Poisson coefficient between both directions perpendicular to the fiber direction.

side of the connection, was simulated by deactivating the cohesive behavior in this region. The full model is available in [16]. For the post-processing and visualization the results were saved in the ASCII format *.fil and were then analyzed with the Python library Pybaqus [15].

4.2 ROTATIONAL STIFFNESS

The numerical results for the moment-rotation behavior are shown in Fig. 15, where both models—with and without simulated failure in region 1—are shown along with the experimental curve. It can be seen that the experimental results yield values in-between the two models, which most probably means that in reality the horizontal faces are not fully unused. The rotational stiffness for the model with and without simulated failure is 7.4×10^2 kNm/rad and 2.3 kNm/rad, respectively. The experimentally measured stiffness is 3.4×10^2 kNm/rad.

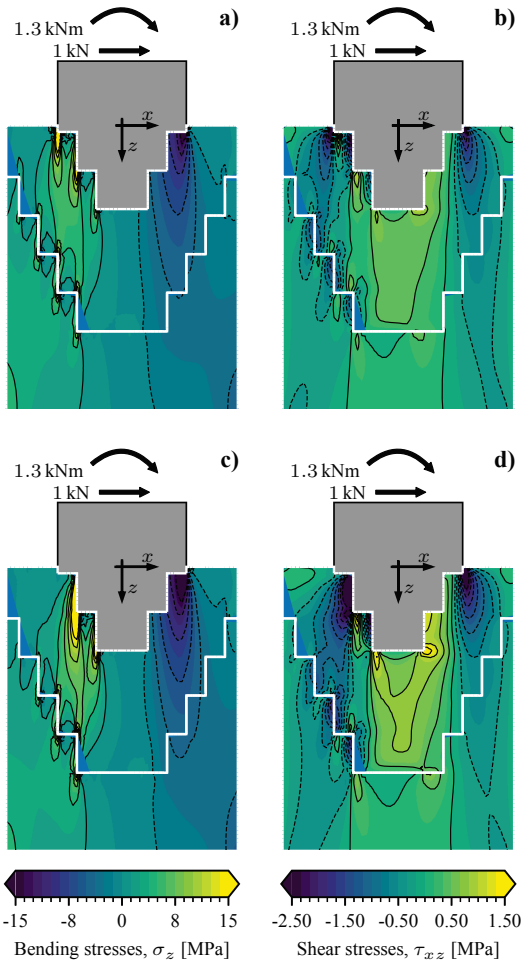

Figure 17: *Stresses in the region of the column-head for the intact connection and with the simulated failure of bonded faces of region 1; (a) Stresses parallel to column axis, σ_z ans (b) shear stresses τ_{xz} for intact connection; (c) Stresses parallel to column axis σ_z and (d) shear stresses τ_{xz} for simulated damaged connection.*

The current analysis did not consider any form of fracture mechanics based softening in the bonded surface, assuming a very simple mixture of cohesive and contact behavior. It can be expected that a much better agreement with the experiments can be obtained, if a more realistic mechanical behavior for the bonded region is used. This could be done by considering softening or by simply adjusting the stiffness properties of the cohesive region.

4.3 STRESSES IN THE COLUMN-HEAD REGION

Figure 17a presents the stresses parallel to the fiber and column axis for the intact model (no failure), where regions of high tensile and compressive stresses are seen at the interface between LVL pin and LVL insert element. The observed asymmetry in the stress distribution is due to the assumption that tensile stresses are not transferred through the horizontally bonded surfaces (endgrain bonding). Figure 17b shows the shear stresses, τ_{xz}, in the same region, where high stressed regions are evidenced on the vertical bond faces on the left side (bending tension side).

Figures 17c,d present the analog results for the model with the simulated failure in region 1. It is evident that the stresses increase significantly due to the reduced cross-section. These high stresses remain mostly in the LVL insert element. From Fig. 17d it can be seen that the shear stresses on the bonded surface are above 2.5 MPa with a moment of 1.4 kN m directly on the top face of the insert element. The characteristic shear strength of the used beech material is 4.5 MPa, which explains the observed failure during the experiments (at about 2.5 kN m).

5 DISCUSSION

5.1 GEOMETRY OF THE CONNECTION

The initial development of the presented connection considered only the effects of vertical loads, as the horizontal loads were assumed to be taken by a stiffening element, such as a reinforced concrete core. However, unless a pin joint is used, some amount of moment will still be transferred to the columnhead, in which case it is important to understand the behavior under moment action, thus justifying this analysis. The most evident problem with the current geometry is the small depth of the vertical step of region 1, which leads to a rather early failure due to the small available shear surface to transfer the stresses. A simple solution for an improvement is to make the first step deeper, hence, increasing the shear surface and resulting in a more robust concept.

5.2 UTILIZED ADHESIVE

Although the bonding of the different components worked very good—as can be judged from the observed axial compression experiments from [17]—, the aspect of the shear failure from Fig. 13 hints a possible limitation of the chosen two-component PUR adhesive. This is due to the rather low percentage of fiber breakage observed. However, it must be stated that the used beech LVL cannot be judged by the same parameters as e.g. softwoods, due to the marked differences in strengths of both materials. Further studies with different gap-filling adhesives should be performed in order to better assess the here presented results.

6 CONCLUSIONS AND OUTLOOK

The current state of a new column-to-column connection was presented. Following one of the project's objective of only using wooden materials if possible, a concept based on softwood GLT and beech LVL was conceived, where the GLT column head is reinforced by embedding a stepped beech LVL insert. Relevant aspects of the mechanical behavior as well as of the manufacture process were presented and discussed, from which the following conclusions can be distilled:

1. The robotic-based manufacturing process proved to be suitable for the precise milling of components with tight tolerances of about 1 mm, enabling the experimental testing of the concept.

https://doi.org/10.52202/069179-0094

2. The rotational stiffness was shown to lay within the range predicted by finite element simulations if damage in region 1 (top most level) is assumed. An improved agreement with the experiments could be achieved by using more realistic material behavior such as softening.

3. The data acquisition during the experiment was problematic due to the rather low fracture load level (about 2 kN) as compared to the maximum load of the machine (1.6 MN). Further experiments will consider a separate load measuring cell, appropriate for the expected load range.

4. The observed failure mode on the shear surface indicates possible limitations with the chosen two-component PUR, which needs to be further assessed experimentally.

5. Finally, although the current geometry is rather weak under bending induced by lateral loading, simple modifications to the geometry can be introduced to improve this if needed.

ACKNOWLEDGEMENTS

The presented ongoing research is partially supported by the Deutsche Forschungsgemeinschaft (DFG, German Research Foundation) under Germany's Excellence Strategy – EXC 2120/1 – 390831618. The authors owe many thanks to the company Pollmeier (Creuzburg, Germany) for generously sponsoring the beech LVL plates (Baubuche) for the presented tests. Further gratitude is owed to the Company Henkel AG & Co. KGaA, Düsseldorf, Germany for supporting the project with tailor-made adhesives.

DATA AVAILABILITY

Some or all data, models, or code generated or used during the study are available in a repository or online in accordance with funder data retention policies. (doi: 10.18419/darus-3388, Ref. [16])

REFERENCES

[1] Abaqus v2022. *ABAQUS/Standard User's Manual, Version 2020*. Providence, RI, USA: Dassault Systèmes, 2022.

[2] R. Abrahamsen. "Mjøstårnet – 18 storey timber building completed." In: *Proc. 24. Internationales Holzbau-Forum (IHF)*. Garmisch-Partenkirchen, Germany, 2018.

[3] S. Aicher and L. Höfflin. "Weibull based design approach of round holes in glulam." In: *International Council for Research and Innovation in Building and Construction – Working Commission W18 – Timber Structures*. Colorado, USA, 2003.

[4] N. S. Bergen. "Case study of UBC Brock Commons - construction details and methods." In: *Proceedings of the World Conference on Timber Engineering (WCTE 2016)*. Austria: Vienna University of Technology, Austria, 2016. ISBN: 978-3-903039-00-1.

[5] M. Claus, C. Tapia, and S. Aicher. "Bond line characteristics of new edge connections of cross-laminated timber in the weak direction based on milled profiled connection plates from laminated veneer lumber made of beech." In: *Otto-Graf-Journal* 20 (2021), pp. 39–60. ISSN: 0938-409X.

[6] DOP PM–017–2022. *Pollmeier Furnierwerkstoffe GmbH: Laminated veneer lumber made from beech for non-load bearing, load bearing and stiffening elements – Board BauBuche S and BauBuche Q*. Declaration of Performance. 2022.

[7] EN 14374. *Timber structures – Structural laminated veneer lumber – Requirements*. Brussels, Belgium: European Committee for Standardization, 2004.

[8] EN 338. *Structural timber – Strength classes*. Brussels, Belgium: European Committee for Standardization, 2016.

[9] ETA-06/0009. *Binderholz Brettsperrholz – Massives plattenförmiges Holzbauelement zur Verwendung als tragendes Bauteil in Bauwerken*. European Technical Assessment. Berlin, Germany, 2017.

[10] ETA-19/0700. *SPIDER Connector and PILLAR Connector*. European Technical Assessment. Vienna, Austria: Austrian Insitute of Construction Engineering (OiB), 2020.

[11] P. Fast, B. Gafner, R. Jackson, and J. Li. "Case study: an 18 storey tall mass timber hybrid student residence at the University of British Columbia, Vancouver." In: *Proceedings of the World Conference on Timber Engineering (WCTE 2016)*. Austria: Vienna University of Technology, 2016. ISBN: 978-3-903039-00-1.

[12] R. McNeel et al. "Rhinoceros 3D, Version 6.0." In: *Robert McNeel & Associates, Seattle, WA* (2010).

[13] M. Muster and A. Frangi. "Experimental analysis and structural modelling of the punching behaviour of continuous two-way CLT flat slabs." In: *Engineering Structures* 205 (2020), p. 110046. DOI: 10.1016/j.engstruct.2019.110046.

[14] Pollmeier Furnierwerkstoffe GmbH. *Declaration of Performance No.: PM–005–2018 – Laminated veneer lumber made from beech – Laminated veneer lumber according to EN 14374:2005-02 for non-load bearing, load bearing and stiffening elements*. Austrian Institute of Construction Engineering. Viena, Austria, 2018.

[15] C. Tapia. *Pybaqus: A Python library for the visualization and post-processing of Abaqus ASCII result files*. Version 0.2.9. 2023. URL: https://github.com/cristobaltapia/pybaqus.

[16] C. Tapia. *Replication Data for: Rotational stiffness of newly developed LVL-based column-head reinforcement for point-supported slab-column building systems*. Version V1. 2023. DOI: 10.18419/darus-3388.

[17] C. Tapia and S. Aicher. “Numerical and experimental investigations on a new concept for column-to-column connections for multi-storey timber buildings.” In: *Materials and Building Construction* (2023). In review.

[18] C. Tapia, L. Stimpfle, and S. Aicher. “A scalable column-CLT-slab connection for open-plan high-rise timber buildings.” In: *Proceedings of the World Conference on Timber Engineering (WCTE 2021)*. Santiago, Chile, 2021.

[19] Z-9.1-775. *Technical Approval, Brettschichtholz mit dem Keilstoß-System “Hess Limiteless” für tragende Holzkonstruktionen – Approval holder: Hasslacher Holding GmbH*. Berlin, Germany: issued by Deutsches Institut für Bautechnik, 2020.

https://doi.org/10.52202/069179-0094